EAGE

Towards a near-surface velocity model of Groningen using transdimensional Markov chains

Rahimi Dalkhani A [1], Ruigrok E [2,3], Weemstra C [1,3]
[1] Department of Geoscience and Engineering, Delft University of Technology, Delft, Netherlands
[2] Department of Earth Sciences, Utrecht University, Utrecht, Netherlands
[3] Seismology and Acoustics, Royal Netherlands Meteorological Institute, De Bilt, Netherlands

Summary

A reliable near-surface velocity is of great importance for seismic hazard analysis and hypocenter location estimation. In this paper, we use transdimensional Markov chain Monte Carlo to infer near-surface shear wave velocity structure from interferometric responses between borehole receivers in the Groningen area. By naturally preferring simple models over more complex models, the algorithm is able to better estimate the depth of an interface, provided only a few velocity interfaces exist. In addition, it provides us with an estimate of the variance of the recovered velocity model.

New Aspects: Using transdimensional tomography to recover shallow velocity structure of the Groningen area based on interfrometric responses of borehole seismic network.

Introduction

The Groningen gas field is the largest gas field in Western Europe. For almost 30 years now, the region has witnessed earthquake activity attributed to the extraction of the gas. The increase in both frequency and magnitude of the induced seismic events has had, and still has, a severe social impact on the region (Van der Voort and Vanclay, 2015). In order to quantify seismic hazard, an accurate shallow velocity model is of great importance (e.g., Kruiver et al., 2017). Also, an improved near-surface velocity model will result in more accurate hypocenter locations (e.g., Spetzler and Dost, 2017). For this reason, a dense seismic network of 70 shallow geophone strings has been installed in the Groningen region (Nederlandse Aardolie Maatschappij, 2016; Figure 1a). Using travel-time picks of virtual-source responses obtained through the application of passive seismic interferometry, Hofman et al (2017) recently derived a compressional and shear-wave velocity profile of this area. For this purpose, these authors used four interferometric travel times, each associated with an interferometric response between the surface receiver and a different borehole geophone. In this study, we show that using more receiver combinations (resulting in 10 interferometric responses), in combination with a transdimensional Markov-chain Monte Carlo (McMC) approach, has its merits.

Compared to conventional McMC algorithms (e.g, 'Metropolis Hastings'), transdimensional McMC is an improvement in the sense that it allows for jumps in the dimensionality of the model. In this study, we use transdimensional Markov chains for the purpose of one-dimensional seismic tomography. In seismic tomography, in general, a set of measurements is used to infer some internal physical properties (e.g. velocity, density, composition, temperature). Conventional (deterministic) tomographic algorithms, however, require proper parametrization and regularization (Tarantola, 2005). Bodin and Sambridge (2009) introduced transdimensional McMC for the purpose of seismic tomography, which is a self-parametrizing algorithm with a naturally smooth result, and which doesn't require any (somewhat arbitrary) regularization. The model space is partitioned by a given number of non-overlapping regions (we call them 'cell'). The number of cells, their location, and their seismic velocities are considered as unknowns in the estimation process. That is, the size, location, and number of cells associated with the most probable velocity model are directly inferred from the data.

Groningen passive borehole data

Figure 1a shows the location of the 70 different borehole stations in Groningen borehole seismic network. Figure 1b shows the station configuration associated with each borehole, which consists of an accelerometer at the surface and a string of four 4.5 Hz geophones with a vertical spacing of 50 m below it (Hofman et al., 2017). For each borehole, Hofman et al (2017) estimated local P and S wave velocities using seismic interferometry (Wapenaar et al., 2010). Figures 1c-f depict the S wave results of their approach for borehole G30, which involves summing cross correlations of transverse components over a large number of local events ($M_L > 1.5$). As such, virtual sources are created at four different depth levels. The red dots in Figure 1c-f indicate the upgoing shear wave travel-time picks that we used for our 1D transdimensional tomography. This study is merely a proof of concept: we anticipate to apply the presented method to all 70 borehole stations in the near future.

Transdimensional seismic tomography

In our case, the forward tomographic problem involves the computation of the travel time t_j associated with a one-dimensional ray j according to (Bodin and Sambridge, 2009):

$$t_j = \sum_{i=1}^{n} \frac{L_{ij}}{v_i}, \qquad (1)$$

where L_{ij} is the length of ray j across cell i, v_i is the velocity value assigned to cell i, and n is number of cells the ray crosses through. Note that for our 1D problem, a cell can be considered a horizontal geological layer with a specific velocity. Consequently, a specific model $\mathbf{m}$ consists of a stack of layers with a specific velocity. The inverse problem involves finding a velocity model $\mathbf{m}$ such that the predicted data $\mathbf{g}(\mathbf{m})$ fits the observed travel times $\mathbf{d}_{\text{obs}}$ as closely as possible. The agreement between observed and predicted data can be quantified by a misfit function such as the weighted least-squares misfit (Bodin and Sambridge, 2009):

$$\emptyset(\mathbf{m}) = \left\| \frac{\mathbf{g(m)} - \mathbf{d_{obs}}}{\boldsymbol{\sigma_d}} \right\|^2, \quad (2)$$

where $\boldsymbol{\sigma_d}$ contains the uncertainties associated with the observed travel-times. Equation 2 implies that the uncertainty σ_j determines how the difference between the measured travel time and the predicted travel time t_j is weighed.

The objective of Bayesian inference is to recover the posterior probability, $p(\mathbf{m}|\mathbf{d}_{\text{obs}})$ from the observed data. Based on the Bayes' rule (Bayes and Price, 1763):

$$p(\mathbf{m}|\mathbf{d}_{\text{obs}}) = \frac{p(\mathbf{d}_{\text{obs}}|\mathbf{m})p(\mathbf{m})}{p(\mathbf{d}_{\text{obs}})}, \quad (3)$$

where $p(\mathbf{m})$ is the prior and $p(\mathbf{d}_{\text{obs}}|\mathbf{m})$ is the likelihood function. Since the evidence, $p(\mathbf{d}_{\text{obs}})$, is not a function of any particular model $\mathbf{m}$, the posterior probability is proportional to $p(\mathbf{d}_{\text{obs}}|\mathbf{m})p(\mathbf{m})$. The likelihood function $p(\mathbf{d}_{\text{obs}}|\mathbf{m})$ can be considered as a measure of agreement between observed and predicted data. For a simple least-squares misfit (Equation 2), the likelihood function is Gaussian (Bodin and Sambridge, 2009):

$$p(\mathbf{d}_{\text{obs}}|\mathbf{m}) \propto \exp\left(-\frac{\emptyset(\mathbf{m})}{2}\right). \quad (4)$$

By assuming independent parameters, the prior can be written as (Bodin and Sambridge, 2009):

$$p(\mathbf{m}) = p(n)p(\mathbf{c}|n)p(\mathbf{v}|n), \quad (5)$$

where n is the number of model parameters or cells, $p(n)$ is the prior on the number of cells, $p(\mathbf{c}|n)$ is the prior on cell nuclei location, and $p(\mathbf{v}|n)$ is the prior on cell velocity.

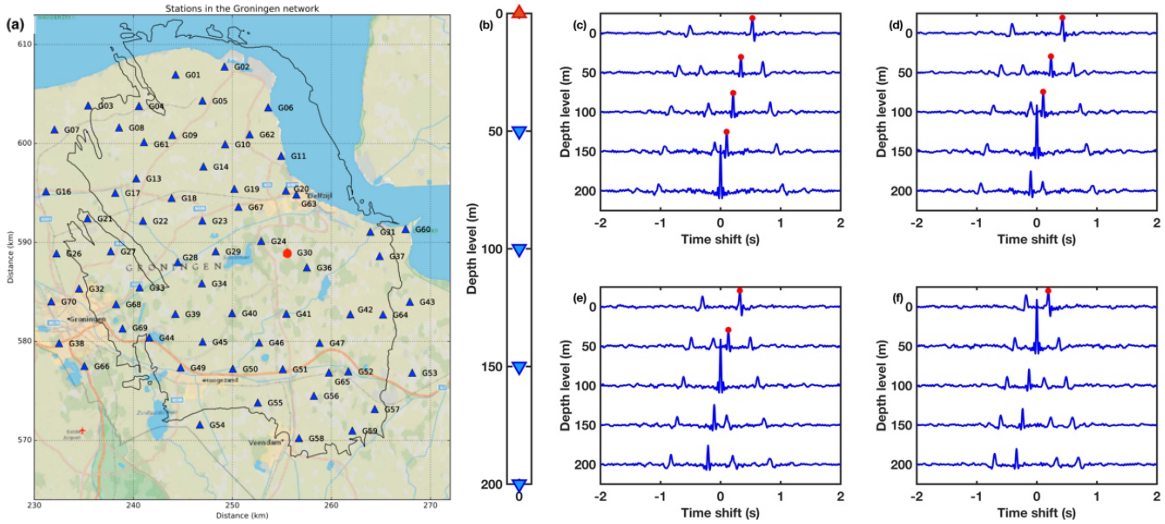

Figure 1 *(a) Map of the borehole stations of the Groningen network. The red filled circle is the borehole we used in our study, G30. (b) Accelerometer (red triangle) and geophones (blue inverted triangle) borehole set up in Groningen. (c-f) Stacks of transverse component cross correlations for virtual sources at different depth levels. The red dots are the travel time picks of upgoing direct S wave that we used in our transdimensional tomography.*

The transdimensional Markov chain draws samples from the posterior distribution by means of an iterative stochastic process. The process starts with a random initial model ($\mathbf{m}$). Then, the algorithm draws the next sample of the chain by proposing a new model, $\mathbf{m'}$, based on a known proposal probability function, $q(\mathbf{m'}|\mathbf{m})$, which only depends on the previous model $\mathbf{m}$. The proposal probability function can be any desired function such as a Gaussian distribution. The proposed sample, then, will be accepted or rejected based on an acceptance ratio for the proposed model, $\mathbf{m'}$ (Bodin and Sambridge, 2009):

$$\alpha(\mathbf{m'}|\mathbf{m}) = \min\left[1, \frac{p(\mathbf{m'})}{p(\mathbf{m})} \times \frac{p(\mathbf{d}_{\text{obs}}|\mathbf{m'})}{p(\mathbf{d}_{\text{obs}}|\mathbf{m})} \times \frac{q(\mathbf{m}|\mathbf{m'})}{q(\mathbf{m'}|\mathbf{m})} \times |\mathbf{J}|\right], \quad (6)$$

where $\mathbf{J}$ is the Jacobian matrix, which accounts for (potential) differences in dimensionality between $\mathbf{m}$ and $\mathbf{m'}$ (i.e., a different number of cells). The pointwise-averaged velocity of the accepted models

(excluding burn-in models) results in the desired smooth solution (Bodin and Sambridge, 2009). From the ensemble of models, i.e., the posterior distribution, the associated pointwise variance can also be computed.

Results and discussion

Figure 2a depicts the source-receiver configuration corresponding to the travel-times of the virtual source responses in Figure 1c-f, which are the upgoing first arrival S-waves. To exemplify the McMC approach detailed above, we consider four different (simple) synthetic velocity models (Figure 2b-e; solid black lines). First, we consider a homogenous velocity model (Figure 2b). The least squares result, the pointwise averaged velocity model (excluding burn-in models), and the most probable model coincide in this case. The confidence intervals are obtained by adding and subtracting the pointwise variance from the pointwise average. For the homogeneous velocity model, the variance slightly changes with depth. The observed increase in variance close to the top and bottom of the model can be explained by the fact that a different number of rays cross each receiver-receiver depth level (from top to bottom, 4, 6, 6, 4, respectively).

Second, we consider two two-layer models (Figure 2c-d). The pointwise averaged velocity profiles are naturally smooth and close to the actual velocity model. The least squares result, however, is not smooth and is also unnecessary complex and far from the true velocity model. The fact that the transdimensional McMC approach is able to correctly determine the depth of the interface can predominantly be explained by the preference of simpler models over more complex models, which is enforced by the prior. The dashed cyan profiles in Figure 2b-e represent the model in the Markov chain with the minimum misfit. Not surprisingly, for the limited number of travel times and the simple synthetic models considered here, these are close to the actual model.

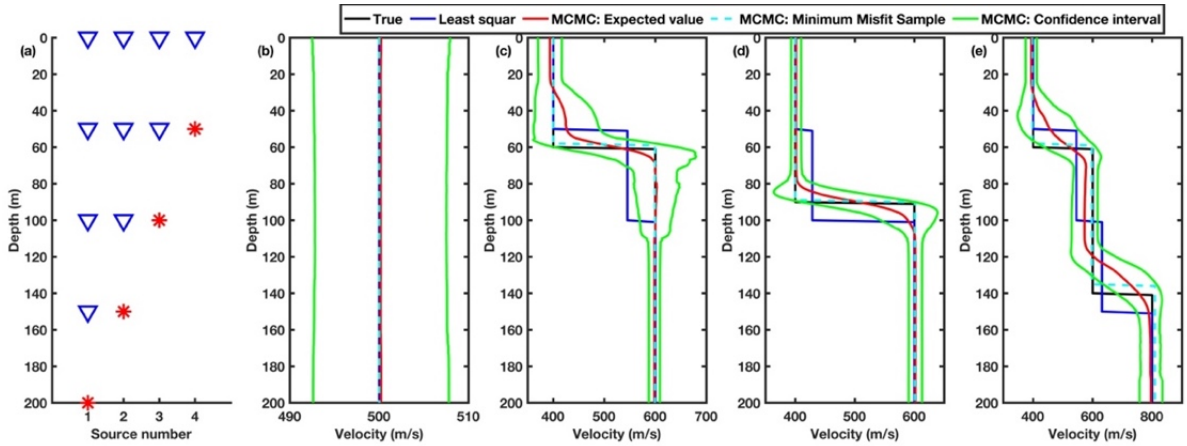

Figure 2 *(a) Source-receiver configuration of the Groningen wells. Triangles and stars depict receivers and virtual sources, respectively. (b-e) Comparison of the pointwise-averaged velocity profile (solid red lines) the least squares results (solid blue lines), and the most probable velocity model of the posterior distribution (dashed cyan lines), with the true velocity model (black solid line). The green curves are the confidence intervals (i.e., the variance) of the models occupying the posterior distribution.*

Figure 3 shows the results of transdimensional McMC to one borehole station over the Groningen gas field, G30. Apart from the synthetic input model, Figure 3a presents the same profiles as depicted in Figure 2b-e. The least-squares method results in a four-layer model, which are of course simply the four receiver-receiver depth levels. The transdimensional McMC result, however, estimates a two-layer model with an interface in depth of around 60 meters, which is the simplest model that fits the data best. It should be understood that the nature of the data is such (receiver increments of 50 meters) that our approach won't able to recover rapidly varying alterations of velocity (e.g., two velocity changes within one of the 50-meter receiver-receiver interval). Figure 3b shows the pointwise variance of all sampled models by McMC. The variance is high at depth ranges where a (large) velocity increase needs to be imposed to fit the travel-times. Figure 3c shows the model density as a function of velocity and depth. Figure 3d shows the sampled velocity as a function of iteration number and depth, which exemplifies how McMC samples the posterior distribution.

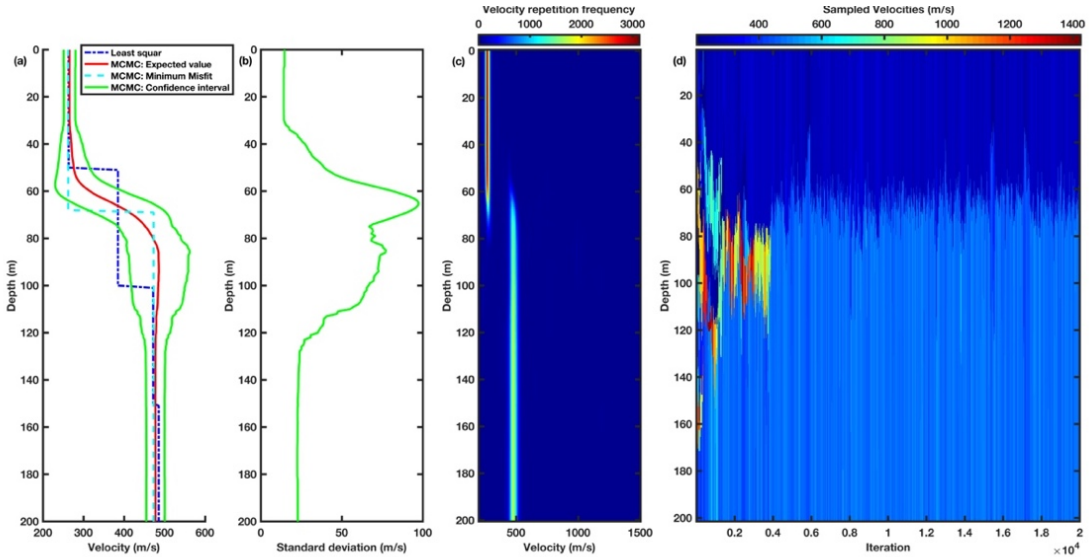

Figure 3 *(a) Results for seismic station G30 (indicted in red in Figure 1). (b) Pointwise variance of the velocity profile. (c) Velocity density as a function of depth (excluding burn-in models). (d) Posterior samples (i.e., velocity models) generated by the transdimensional Markov chain.*

Conclusions

In this paper, we investigated the ability to recover near-surface velocities using transdimensional Markov chains. The transdimensional tomographic problem is solved in one dimension by using interferometric travel times between different borehole receivers. For models with few interfaces, the pointwise average of the posterior distribution provides a reliable estimate of the true velocity structure. In addition, confidence intervals can be obtained by computing the pointwise variance of the ensemble of model constitution the posterior distribution. As a field-data proof of concept, we used the transverse components of a single borehole in the Groningen region to infer shear wave velocities in the top 200 meters.

References

Bayes, M. and Price, M. [1763] An essay towards solving a problem in the doctrine of chances. By the late Rev. Mr. Bayes, F. R. S. communicated by Mr. Price, in a letter to John Canton, *A.M.F.R.S. Philosophical Transactions*, 53, 370–418.

Bodin, T. and Sambridge, M. [2009] Seismic tomography with the reversible jump algorithm. *Geophysical Journal International*, **178**(3), 1411-1436.

Hofman, L.J., Ruigrok, E., Dost, B. and Paulssen, H. [2017] A shallow seismic velocity model for the Groningen area in the Netherlands. *Journal of Geophysical Research: Solid Earth*, ***122***(10), 8035-8050.

Kruiver, P.P., van Dedem, E., Romijn, R., de Lange, G., Korff, M., Stafleu, J., Gunnink, J.L., Rodriguez-Marek, A., Bommer, J.J., van Elk, J. and Doornhof, D. [2017] An integrated shear-wave velocity model for the Groningen gas field, The Netherlands. *Bulletin of Earthquake Engineering*, **15**(9), 3555-3580.

Nederlandse Aardolie Maatschappij [2016] Study and Data Acquisition Plan Induced Seismicity in Groningen.

Spetzler, J. and Dost, B. [2017] Hypocentre estimation of induced earthquakes in Groningen. *Geophysical Journal International*, **209**(1), 453-465.

Tarantola, A. [2005] Inverse problem theory and methods for model parameter estimation (Vol. **89**). *SIAM*.

Van der Voort, N. and Vanclay, F. [2015] Social impacts of earthquakes caused by gas extraction in the Province of Groningen, The Netherlands. *Environmental Impact Assessment Review*, **50**, 1-15.

Wapenaar, K., Draganov, D., Snieder, R., Campman, X. and Verdel, A. [2010] Tutorial on seismic interferometry: Part 1—Basic principles and applications. Geophysics, **75**(5), 75A195–75A209.